Available online at www.sciencedirect.com
SCIENCE DIRECT®
International Journal of Heat and Fluid Flow 26 (2005) 362–377
International Journal of HEAT AND FLUID FLOW
www.elsevier.com/locate/ijhff

Vortex interactions in a two side-by-side cylinder near-wake

Z.J. Wang, Y. Zhou *

Department of Mechanical Engineering, The Hong Kong Polytechnic University, Hung Hom, Kowloon, Hong Kong

Received 22 September 2004; accepted 29 October 2004
Available online 30 December 2004

Abstract

The flow behind two side-by-side circular cylinders is experimentally investigated based on laser-illuminated flow-visualization, particle image velocimetry and hot-wire measurements. The flow is classified as three regimes: single street (the cylinder center-to-center spacing $T/d < 1.2$), asymmetrical flow ($1.2 < T/d < 2.0$) and two coupled street ($T/d > 2.0$). Special attention is given to the regime of $1.2 < T/d < 2.0$, which is characterized by one narrow and one wide wake. It is found that the flow structure and its downstream evolution are closely linked to the phase relationship between the gap vortex in the wide wake and that in the narrow wake. When the gap vortex in the wide wake leads in phase, the two opposite-signed vortices in the narrow wake are typically engaged in pairing, which yields a relatively low-pressure region between them, thus drawing in the gap vortex along with fluid in the wide wake. This vortex interaction may act to stabilize the gap flow deflection. When lagging behind in phase, the gap vortex in the wide wake fails to merge with the vortices in the narrow wake. Interactions between vortices in the two wakes lead to the changeover of the gap flow deflection from one side to another. It is further noted that, for $L/d > 2.0$, the flow structure change from the anti-phase to in-phase mode starts with a phase shift between gap vortices. The dynamical role of gap bleeding between cylinders for $L/d < 1.2$ is also examined.

Keywords: Interacting wakes; Vortex streets; Vortex interactions

1. Introduction

Flow around two side-by-side cylinders has received considerable attention in the past (Bearman and Wadcock, 1973; Zdravkovich, 1977; Williamson, 1985; Kolář et al., 1997; Sumner et al., 1999) because of its inherent importance and practical significance in many branches of engineering. This flow depends to a great extent on the ratio T/d (T is the center-to-center cylinder spacing and d is the cylinder diameter) among many other parameters, e.g. initial conditions, pressure gradient and Reynolds number.

For $T/d > 2$ two distinct vortex streets occur (Landweber, 1942). The two streets are coupled, with a definite phase relationship (Kim and Durbin, 1988); they are characterized by a single frequency (Spivac, 1946). This frequency was further found to be the same as the frequency measured in the single cylinder wake. Using a Schlieren optical method, Ishigai et al. (1972) observed a remarkably symmetric vortex formation and shedding for $T/d = 2.5$ and 3.0. Based on flow-visualization data at the Reynolds number Re ($\equiv U_\infty d/\nu$, where ν is the kinematic viscosity) = 100–200, Williamson (1985) demonstrated that the two streets may occur either in phase or in anti-phase. In this paper, 'antiphase' means vortex shedding, symmetrical about the flow centerline, from the two cylinders and 'in-phase' refers to anti-symmetric vortex shedding. The in-phase streets eventually merged downstream to form a single street, while the in–anti-phase streets remained distinct farther downstream. He observed a predominant antiphase vortex shedding for $2 < T/d < 6$. These studies have greatly improved our

* Corresponding author. Tel.: +852 2766 6662; fax: +852 2365 4703.
E-mail address: mmyzhou@polyu.edu.hk (Y. Zhou).

0142-727X/$ - see front matter © 2004 Elsevier Inc. All rights reserved.
doi:10.1016/j.ijheatfluidflow.2004.10.006

understanding of the flow behind two side-by-side cylinders for relatively large T/d (>2). However, some aspects of the flow have yet to be clarified. For example, what triggers the transition of the two vortex streets from the in–antiphase to the in-phase mode?

At an intermediate cylinder spacing, i.e. $1.2 < T/d < 2.0$, the interaction between the wakes associated with the two cylinders is expected to intensify; the gap flow between the cylinders is deflected, forming one narrow and one wide wake. It has been found that the vortex frequency associated with the narrow wake approximately triples that for the wide wake (Bearman and Wadcock, 1973; Sumner et al., 1999). The deflected gap flow may change over intermittently from one side to another and is bi-stable. The bi-stability is nominally independent of the Reynolds number (Kim and Durbin, 1988). Nevertheless, a number of important issues have yet to be clarified of the asymmetric flow regime. Typically, physics behind the formation and stability of a narrow and a wide wake is unclear. Furthermore, what triggers the changeover of the gap flow deflection from one side to another? Why does the dominant frequency in the narrow wake triple that in the wide wake? How do the vortices in both wakes evolve downstream?

At very small spacing, i.e. $T/d < 1.2$, no vortex is generated in the gap between the cylinders; vortices are alternately shed from the free-stream side only of the two cylinders, generating a single vortex street. Sumner et al. (1999) noted that the alternate vortex shedding was supplanted from time to time by the symmetric shedding. They further pointed out that gap bleeding was usually associated with higher momentum, acting to increase the streamwise extent of the vortex formation region. However, the possible role gap bleeding plays in vortex formation and downstream evolution has not been thoroughly investigated.

The present work aims to address the issues raised above based on flow visualization, particle image velocimetry (PIV) and hot-wire measurements in order to gain a better understanding of the vortex generation, interaction and downstream evolution in the three different flow regimes. Special attention is given to the asymmetrical flow regime ($T/d < 2.0$), including the stability of the deflected gap flow, its random changeover from one side to another and vortex generation mechanisms. The role gap bleeding plays in the vortex formation and downstream development for very small spacing between the cylinders is examined in detail.

2. Experimental details

2.1. Laser-induced fluorescence (LIF) flow visualization

Experiments were carried out in a water tunnel. The square working section ($W \times H \times L = 0.15\ \text{m} \times 0.15\ \text{m} \times 0.5\ \text{m}$) is made up of four 20 mm thick Perspex panels. The maximum flow speed in the working section is about 0.32 m/s. More details of the tunnel were given in Zhou et al. (2001).

Two side-by-side acrylic circular tubes of an identical diameter of $d = 10$ mm were horizontally mounted 0.20 m downstream of the exit plane of the tunnel contraction and placed symmetrically about the mid-plane of the working section. They spanned the full width of the tunnel, resulting in a blockage of 13.3%. Three transverse spacing ratios were used, i.e., $T/d = 3.00$, 1.70 and 1.13, respectively, each being representative of different proximity effects for two side-by-side circular cylinders (Zdravkovich, 1985).

Dye (Rhodamine 6G 99%) was chosen to be the flow marker, which had a faint red color and became metallic green when excited by laser. For each cylinder, dye was introduced through two injection pinholes of 0.5 mm in diameter at the mid-span of the cylinder. The two pinholes were located at 90°, clockwise and anti-clockwise, respectively, from the forward stagnation point. A thin laser sheet, which was generated by laser beam sweeping, provided illumination vertically at the mid-plane of the working section. A Spectra-Physics Stabilite 2017 Argon Ion laser with a maximum power output of 4 W was used to generate the laser beam. A digital video camera recorder (Sony DCR-PC100E) was used to record the dye-marked vortex street at a framing rate of 25 fps. Since flow visualization was conducted at a relatively small Re ($\equiv U_\infty d/\nu = 120$–$1100$, where U_∞ and ν are the free-stream velocity and the kinematic viscosity of fluid, respectively), the framing rate provided sufficient resolution to investigate the vortex motion. For example, for each time interval (1/25 s) between consecutive frames, vortices were convected for about $0.21d$ at $Re = 600$ (flow-visualization data will be shown mostly at this Re or lower), which was significantly smaller than the vortex scales. The view window was $x/d \approx 0$–8. The recording duration was typically 10 min.

2.2. Hot-wire measurements

Experiments were carried out in a closed circuit wind tunnel with a 2.0 m long square cross-section of $0.6\ \text{m} \times 0.6\ \text{m}$. Two brass circular cylinders of 12.7 mm diameter, corresponding to an aspect ratio of 47, were installed side-by-side in the mid-plane and spanned the full width of the working section. The cylinders were located at 0.20 m downstream of the exit plane of the contraction, resulting in a maximum blockage of about 4.2%. The Reynolds number Re investigated was 5900. It has been verified at this Re that the mean velocity and turbulence intensities are reasonably uniform across most of the wake for the present cylinder aspect ratio. Therefore, no attempt was made to manipulate the end conditions, although Williamson (1996) and Prasad

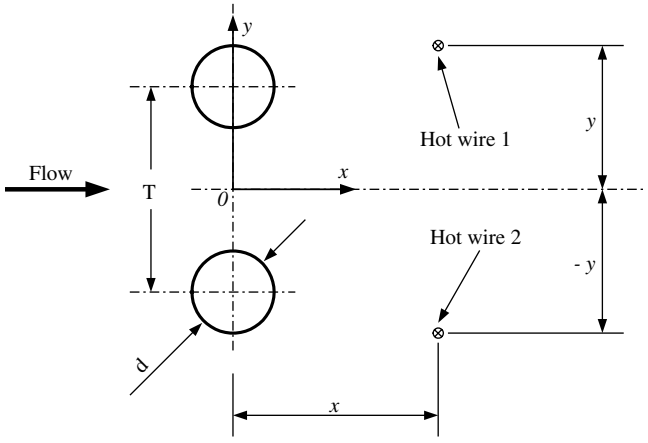

Fig. 1. Experimental arrangement of hot-wire measurements.

and Williamson (1997b)'s investigations indicated that it was possible to control oblique and parallel shedding at *Re* up to 5000. Three transverse spacing ratios, identical to those in flow-visualization investigations, were used. The longitudinal turbulence intensity in the free-stream was measured to be approximately 0.4%. Measurements were carried out over $0 \leqslant x/d \leqslant 10$ and $y/d = 0$ to ± 5.0.

Two single hot-wires were placed symmetrically about the flow centerline, $y/d = 0$ (Fig. 1). Hot-wires 1 and 2, moveable along both x and y directions, measured simultaneously the velocity fluctuations on both sides of the flow centerline. The wires were operated at an overheat ratio of 1.8 on constant temperature circuits. Signals from the wires were simultaneously offset, amplified and then digitized using a 12 bit A/D board and a personal computer at a sampling frequency of 6.0 kHz per channel. The duration of each record was about 20 s.

2.3. PIV measurements

The wind tunnel and other experimental conditions were the same as those used for the hot-wire measurements. A Dantec PIV system, introduced in detail by Xu et al. (2003), was used to obtain quantitative information of the patterns of vorticity. The cylinder surface and the tunnel working section wall hit by the laser sheet were painted black to minimize reflection noises. The flow was seeded by smoke, generated from Paraffin oil, of a particle size around 1 μm in diameter. The digital particle images from the PIV measurement were taken using one CCD camera (HiSense type 13, 1280 × 1024 pixels). Each image covered an area of 127.5 mm × 102 mm, i.e. $x/d = -0.5d$ to $8d$ and $y/d = -3.4d$ to $+3.4d$, corresponding to an image magnification of about 0.1 mm/pixel in both horizontal and vertical directions. Both cylinders, included in the PIV images, were masked using a built-in masking function in the PIV system before particle velocities were calculated. In image processing, 32 × 32 rectangular interrogation areas with 25% overlap in the horizontal and vertical directions, respectively, were used. The spatial resolution for vorticity was thus estimated to be 32 pixels × (1–25%) × 0.1 mm/pixel = 2.4 mm ($\approx 0.19d$). The ensuing in-plane velocity vector field consisted of 53 × 42 vectors. The same number of spanwise vorticity component, ω_z, were approximately derived based on particle velocities.

3. Flow characteristics for large cylinder spacing

Fig. 2 shows the instantaneous vorticity contours $\omega_z^* = \omega_z d/U_\infty$ derived from the PIV measurement of the velocity field at $T/d = 3.00$. The contours display two anti-phase vortex streets about the centerline (Fig. 2). The maximum ω_z^* associated with the inner vortex separating from the cylinder side near $y = 0$ is about 2.3, appreciably smaller than that (2.9) associated with the outer vortex generated from the free-stream side of a cylinder, suggesting that the inner vortices could be weaker than the outer vortices. The results are consistent with previous reports. Kolář et al. (1997) conducted ensemble-averaging of LDA data measured in the near-wake of two side-by-side square cylinders ($x/d < 10$, $T/d = 3.0$, where d is the height of square cylinders) and noted a weak strength and fast decay in inner vortices. They proposed that the interaction between the inner vortices shed from different cylinders was mainly responsible for the fast decay in inner vortices. The present data further suggest that the inner vortices could be shed with smaller circulation, confirming Zhou et al. (2002)'s speculation.

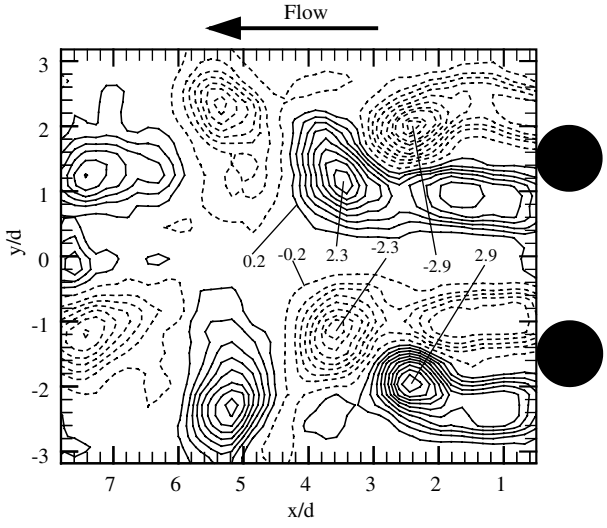

Fig. 2. The instantaneous vorticity contours $\omega_z^* = \omega_z d/U_\infty$ obtained from the PIV measurement. $T/d = 3.00$, $Re = 5900$. The contour increment = 0.28.

The two vortex streets are mostly anti-phased, irrespective of the laminar or turbulent flow regime, as previously reported by e.g. Ishigai et al. (1972), Bearman and Wadcock (1973) and Williamson (1985). However, the in-phase vortex shedding occurs from time to time in the *Re* range investigated. The mode change from anti-phase to in-phase or vice versa is not well understood. Fig. 3 shows the sequential photographs ($Re = 450$). The real time index is given by the first three numbers on the upper left-hand corner in the photographs and the sequential order is indicated by the fourth number. Initially, vortices were shed in anti-phase (Plate 1). However, the two gap vortices, marked by arrows in Plate 2, were formed with a small phase deviation from the anti-phase vortex shedding. This is not unexpected especially in the context of a turbulent flow since a constant phase shift between the two gap vortices is highly unlikely. The gap vortices are fairly close to and thus interact with each other. Such interaction appears encouraging the formation of staggered vortices. As the vortices grow in size downstream, the interaction is expected to intensify, resulting in an increased phase deviation from the anti-phase mode (Plates 3 and 4). Note that the downstream fluid dynamics may have an upstream influence, which may have an impact upon the initial evolution of the shear layer instability (e.g. Rockwell, 1983; Ho and Huerre, 1984). Michalke (1984) has further suggested that the initial shear layer instability was controlled by downstream vorticity dynamics. It seems therefore plausible that this increased phase deviation (Plates 3 and 4) may feed back upstream, causing following vortices to be shed in phase from the two cylinders (Plates 4 and 5). Eventually, we see the two vortex streets arranged spatially in the in-phase mode (Plate 5). The two vortex streets in the in-phase mode are however less stable and soon become somewhat disorganized; the formation of the upper gap vortex appears suppressed (Plates 6 and 7). The vortex streets revert to the anti-phase mode within two shedding periods (Plates 8 and 9). It may be concluded that, while anti-phase vortex shedding is relatively stable, in-phase vortex shedding, which may be initiated by a small phase deviation between the gap vortices, is unstable.

Weaver and Abd-Rabbo (1984) and Granger et al. (1993) observed a symmetric vortex shedding in a square array of tubes in a cross-flow. Weaver and Abd-Rabbo (1984) proposed that a symmetric-mode jet instability mechanism might have caused or at least triggered this phenomenon. Granger et al. (1993) suggested that the inline cylinder motion caused a symmetric oscillation of separation points at the surface of the moving cylinder and could be responsible for the symmetric vortex shedding. In the present investigation, the inline cylinder

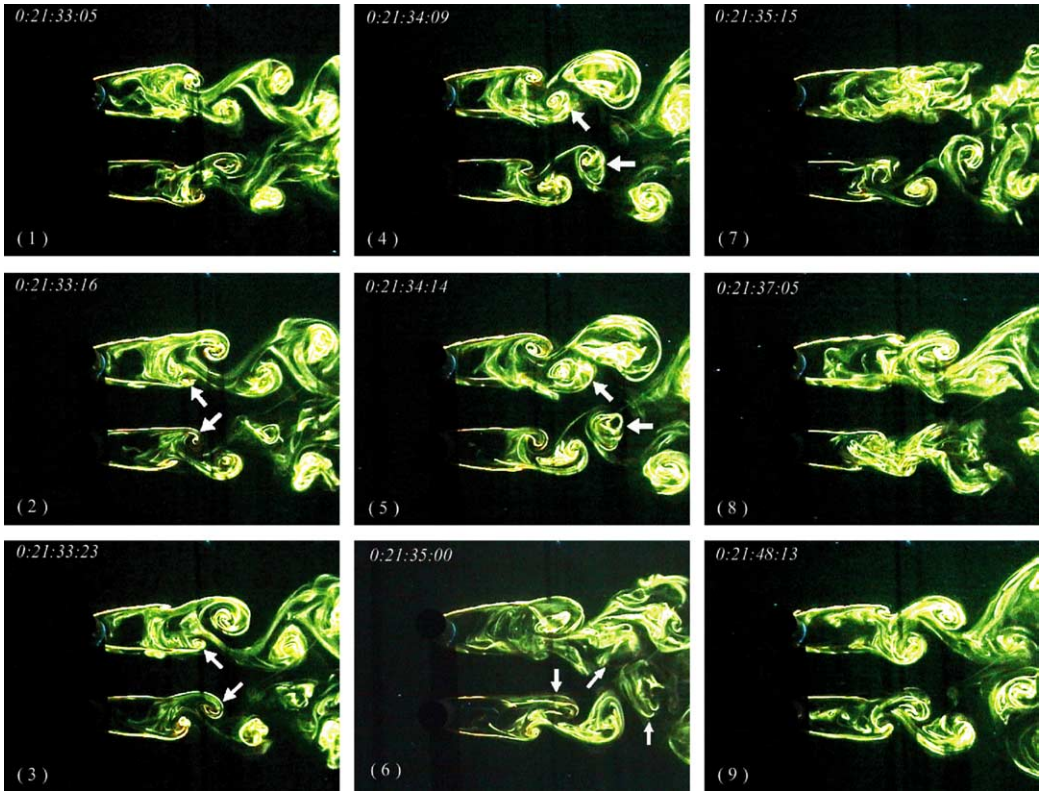

Fig. 3. Sequential photographs from laser-illuminated flow-visualization: transition from the anti-phase to in-phase mode vortex shedding. $T/d = 3.00$, $Re = 450$.

motion is unlikely to be responsible for antiphase vortex shedding since vortex-induced vibration of the cylinders is negligibly small. Relatively stable anti-phase vortex shedding is likely attributed to a possibly symmetric pressure differentiation about the centerline. Zhou et al. (2001)'s pressure measurement around the two cylinders indicated that the pressure upstream of the gap between the cylinders was higher than that close to the free-stream because of flow retardation. They inferred that there was a pressure differentiation on the two sides of each cylinder in the cross-flow direction. The differentiation may be symmetrical with respect to $y/d = 0$, as supported by the numerical calculation of the pressure field around two side-by-side cylinders at $T/d = 3$ and 4 (Meneghini and Saltara, 2001). Such a pressure distribution is likely to suppress in-phase vortex shedding and induce the anti-phase behavior.

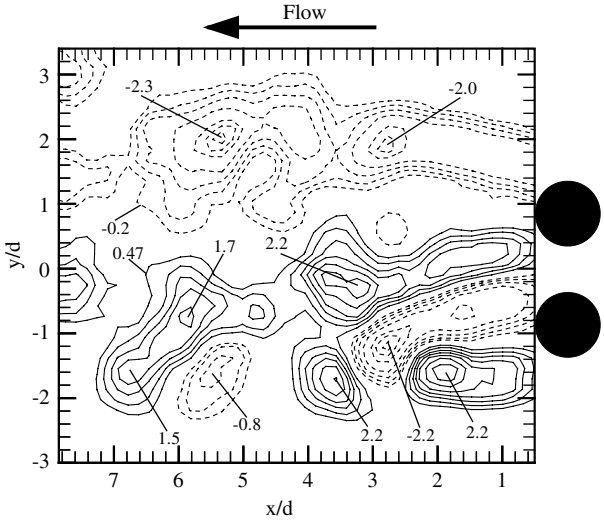

Fig. 4. The instantaneous vorticity contours $\omega_z^* = \omega_z d/U_\infty$ obtained from the PIV measurement. $T/d = 1.70$, $Re = 5900$. The contour increment = 0.29.

4. Asymmetrical flow for intermediate cylinder spacing

In this section, we examine the flow in the asymmetrical regime ($T/d = 1.2$–2.0), focusing on following issues: vortex generation mechanisms, why the gap flow is stably deflected, what causes the changeover of the gap flow from one side to the other and why the dominant frequency in the narrow wake triples that in the wide wake.

4.1. Different vortex generation mechanisms in the narrow and wide wakes

Vortical structures in the narrow wake behave very differently from those in the wide wake. For example, the former and the latter are associated with high and low vortex frequencies, respectively (Spivac, 1946; Ishigai et al., 1972; Bearman and Wadcock, 1973; Kamemoto, 1976; Kiya et al., 1980; Kim and Durbin, 1988; Sumner et al., 1999). Some researchers (Kim and Durbin, 1988; Sumner et al., 1999) referred to the frequencies as vortex-shedding frequencies. It is of fundamental interest to understand thoroughly the generation mechanisms of the vortical structures.

Fig. 4 presents the typical ω_z^*-contours at $T/d = 1.70$ deduced from PIV measurements. The gap flow is deflected towards the lower cylinder, resulting in one narrow (lower) and one wide (upper) wake. The vortical structures in the wide wake start to occur at about $x/d = 3$. In contrast, those in the narrow wake are visible at about $x/d = 1.8$. In addition, the maximum magnitude of ω_z^* in the wide wake is initially 2.0, smaller than that (2.2) in the narrow wake. Further downstream, however, this magnitude increases to 2.3 in the wide wake but decreases considerably in the narrow wake. Evidently, the vortical structures in the narrow wake behave very differently from those in the wide wake. Beyond $x/d = 6$, the two streets appear merging into one.

Fig. 5a shows the downstream evolution of the power spectrum E_u in the wide wake. The most dominant frequency is $f^* \approx 0.1$. Note that vortex rolling-up in the wide wake occurs quite far away from the cylinder (Fig. 6), apparently different from vortex shedding from a cylinder. Furthermore, the peak at $f^* \approx 0.1$ grows downstream, up to about $x/d \approx 10$ (Fig. 5a). This is in distinct contrast with the downstream evolution of the peak at $f^* \approx 0.3$ (Fig. 5b) in the narrow wake, which reaches maximum at $x/d = 1.5$ and then is considerably reduced at $x/d = 5$. By $x/d = 10$, there is no presence of the peak at $f^* \approx 0.3$. The observation from vorticity con-

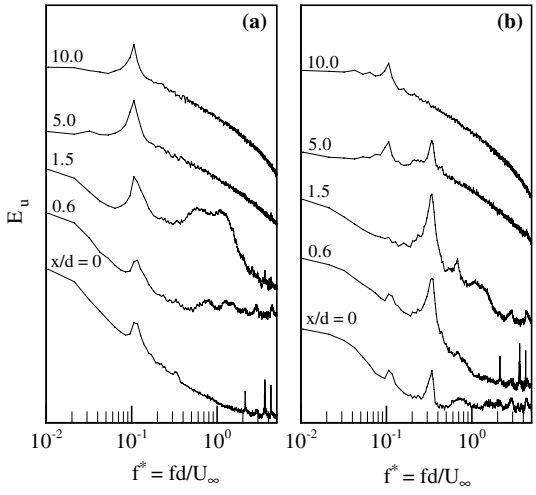

Fig. 5. Downstream evolution of the power spectrum E_u of hot-wire signals simultaneously measured at $y/d = \pm 2.0$: (a) the wide wake; (b) the narrow wake. $T/d = 1.70$. $Re = 5900$.

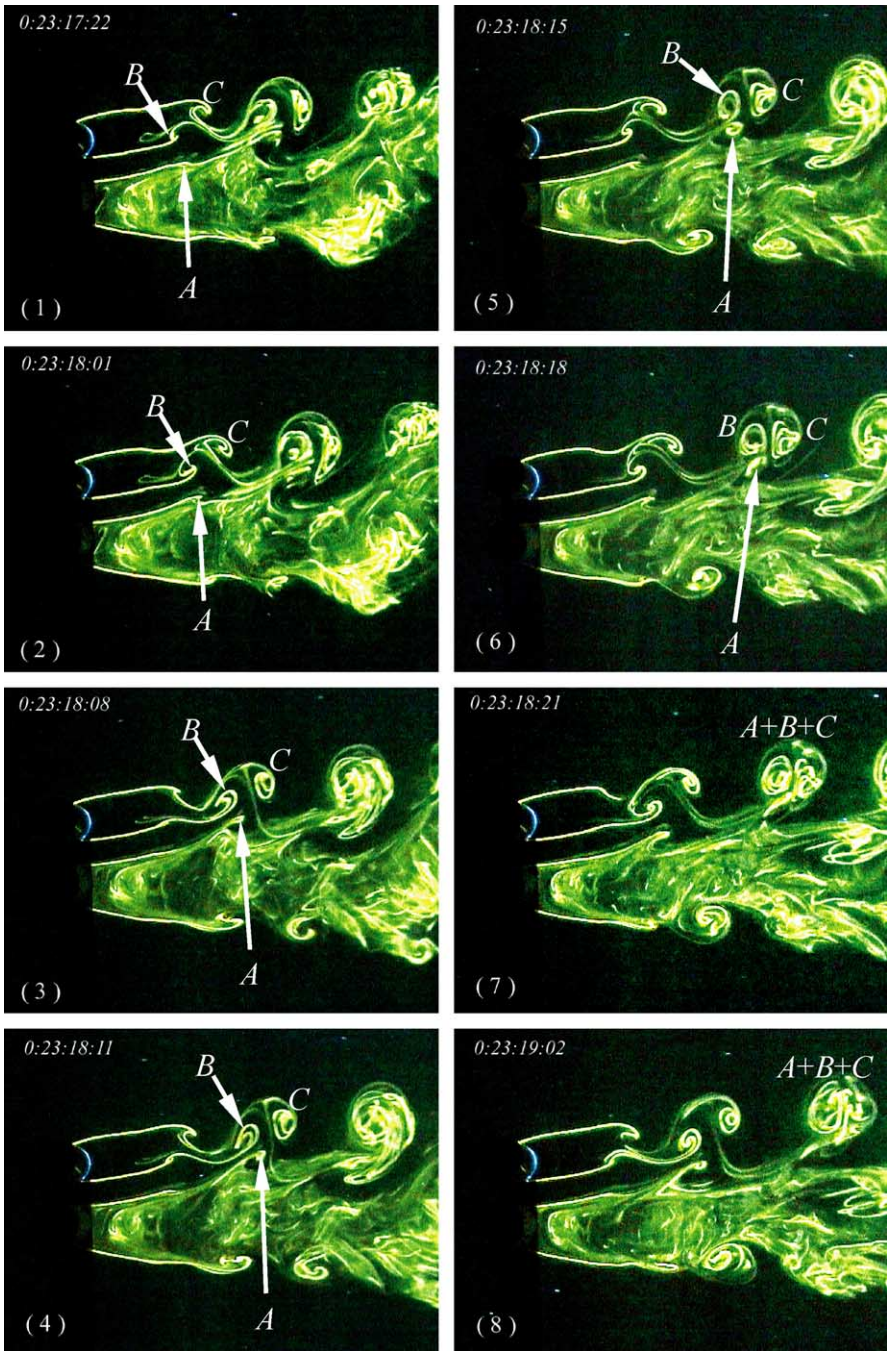

Fig. 6. Sequential photographs from flow-visualization: the pairing opposite-signed vortices B and C in the narrow wake draw in the gap vortex A in the wide wake. $T/d = 1.70$, $Re = 450$.

tours and hot-wire spectra suggest a difference in the generation mechanism between vortices in the narrow and wide wake.

Zhou and Antonia (1994) compared the turbulent near-wakes ($x/d = 10$) generated by a screen of 50% solidity and solid bluff bodies including circular, square and triangular cylinders. They noted a larger $\overline{v^2}$ than $\overline{u^2}$ in the solid body wakes, where $\overline{u^2}$ and $\overline{v^2}$ are the streamwise and lateral Reynolds normal stresses, respectively. However, $\overline{v^2}$ was smaller than $\overline{u^2}$ in the screen wake, resembling a self-preserving turbulent far-wake (Zhou et al., 1998). The observation was linked to a difference in the generation of vortices. While vortices behind a solid body originated from vortex shedding, those in a screen near-wake or the far-wake of a solid body were ascribed to the shear layer instability. Interestingly, the LDA measurements at $x/d = 1.5$ (not shown) indicated that $\overline{v^{2^*}}$ was larger than $\overline{u^{2^*}}$ across the narrow wake

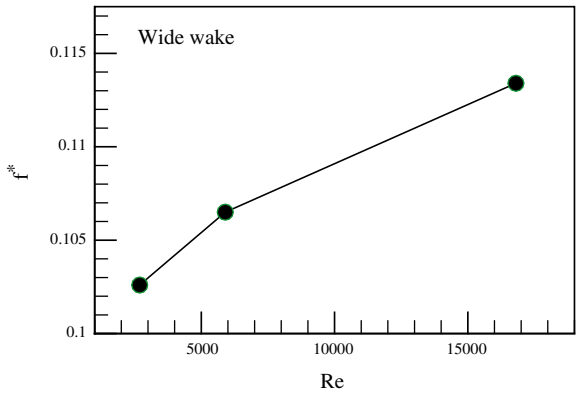

Fig. 7. Dependence on Re of the dominant frequency f^* in the wide wake. The hot-wires were located $x/d = 1.5$ and $y/d = \pm 2.0$. $T/d = 1.70$.

but the other way around across the wide wake. It may be inferred that the vortical structures in the wide wake may originate from rolling-up far away, e.g. about $5d$ at $Re = 5900$ (Fig. 4), from the cylinder under the effect of the shear layer instability. Bloor (1964) related the separating shear layer thickness δ of a cylinder to Re by $\delta \sim 1/\sqrt{Re}$. Presumably, the shear layer thickness in the wide wake is also inversely related to Re, implying a rising dominant frequency f^* for higher Re. This is indeed confirmed in Fig. 7. The proposition is further supported by the variation in the vortex strength, which increases downstream (Figs. 4 and 5a) until the formation process is completed at $x/d \approx 10$. On the other hand, those vortices in the narrow wake are generated from vortex shedding from the cylinder. Accordingly, their strength impairs as x/d increases (Figs. 4 and 5b).

4.2. Stability of gap flow deflection

The gap flow deflection and the formation of wide and narrow wakes behind a row of bluff bodies for $T/d = 1.2$–2.0 have been previously reported (Ishigai et al., 1972; Williamson, 1985; Moretti, 1993). Ishigai et al. (1972) and Moretti (1993) ascribed the gap flow deflection to Coanda effect, that is, an air jet flowing near the wall of the fuselage of an aircraft would deflect so as to flow closer to the wall (Englar, 1975; Sobey, 2000). However, based on the observation of different base pressures, Bearman and Wadcock (1973) inferred a deflected gap flow behind two side-by-side flat plates and thus argued that the gap flow deflection was not caused by the boundary layer separation; instead, it was a near-wake phenomenon. Their argument was further supported by Williamson (1985)'s flow-visualization data, which showed a deflected gap flow behind two side-by-side flat plates. One may surmise that, since a straight flow between abrupt two-dimensional bluff bodies tends to be unstable, the initial deflection of the gap flow may occur due to perturbations such as non-symmetric vortex shedding from the two cylinders. A number of factors may contribute to the stably deflected gap flow.

Firstly, since the two cylinders are relatively close, strong interactions between vortices in the narrow and wide wake may naturally influence the behaviors of the gap flow and contribute to its stable deflection. Fig. 6 presents typical sequential photographs from the LIF visualization ($Re = 450$). Two rows of vortices in the narrow wake appear pushed by the wide wake so that their lateral spacing is very small. Initially, longitudinal spacing between two opposite-signed vortices B and C in the narrow wake is large (Plates 1–3). However, Plates 4 and 5 show diminishing spacing, both longitudinally and laterally, between B and C. It is likely that the gap vortex B travels faster than the outer vortex C, possibly carried by the gap flow jet of a higher mean velocity (Sumner et al., 1999). The two approaching counter-rotating vortices could create a region between them, where the upward lateral velocity is relatively large and pressure being low. Meneghini and Saltara (2001) conducted a numerical study of the flow behind two side-by-side cylinders. At $T/d = 1.5$ ($Re = 200$), the two counter-rotating vortices (their Fig. 15a) in the relatively narrow (lower) wake appeared fairly close. The pressure corresponding to the region between the two vortices (their Fig. 14a) was low and hence drew in fluid from the other wake (their Fig. 15a). The low-pressure region is expected to produce two effects: (1) induce B and C to further approach each other, forming a pair (Plates 5 and 6); (2) draw in the gap vortex as well as fluid in the wide wake. The latter effect is evident from the movement of the gap vortex A in the wide wake, which appears approaching the region between the pairing vortices B and C (Plates 3–6). As a matter of fact, A amalgamates with pairing B and C, eventually resulting in one single structure (Plates 7–8). This observation was found to be quite typical in the Re range presently investigated. It is therefore proposed that the low-pressure region resulting from the pairing vortices in the narrow wake at least partially contributes to the stability of one narrow and one wide wake.

Secondly, as the gap flow is associated with a relatively high momentum, the base pressure behind the cylinder, towards which the gap flow is deflected, should be lower than that behind the other cylinder (Zhou et al., 2001). As a result, the gap flow deflection tends to be stabilized.

Thirdly, the vortices shed from the cylinder in the narrow wake are generally characterized by a high frequency and thus relatively weak strength. For example, the maximum ω_z^* is 2.2 in the narrow wake (Fig. 4), significantly smaller than that (2.9) at $T/d = 3.0$ (Fig. 2); those generated in the wide wake are even weaker, about 2.0 (Fig. 4). Therefore, the fluctuation of the velocity or pressure field could have a limited strength, generally

not strong enough to force the gap flow to change over from one side to another.

A combination of wide and narrow wakes has been observed behind multiple cylinders of various geometrical configurations, for example, a row of cylinders (Moretti, 1993), three side-by-side cylinders of equal (Kumada et al., 1984) and unequal cylinder spacing (Zhang and Zhou, 2001), two staggered cylinders (Sumner et al., 2000). Zhang and Zhou (2001)'s flow visualization clearly showed the amalgamation of the two cross-stream vortices in the narrow wake with the gap vortex in the wide wake. Sumner et al. (2000)'s data (their Fig. 9) also indicated a similar interaction between vortices, though they interpreted that the two gap vortices were pairing, and then enveloped by a vortex in the narrow wake. Such interaction was further observed numerically (Ng et al., 1997). It is speculated that the amalgamation of the three vortices could occur in all the flows composed of a number of narrow and wide wakes.

4.3. Changeover of the gap flow

It is well known that for $1.2 < T/d < 2.0$ the deflected gap flow is bi-stable and intermittently changes over from one side to another (Ishigai et al., 1972; Bearman and Wadcock, 1973; Kim and Durbin, 1988). However, physics behind the changeover is so far not well understood. A close examination of the present flow-visualization data unveils that the changeover is often associated with a phase lag of the gap vortex in the wide wake behind that in the narrow wake.

Fig. 8 presents sequential photographs of the changeover process ($Re = 230$). Initially, the gap flow was deflected upwards (Plate 1). The gap vortices in the two wakes appear in–antiphase, which is rather generic based on present LIF data. The observation may also be inferred from hot-wire signals u_1 and u_2 simultaneously measured at $x/d = 1.5$ and $y/d = \pm 0.4$. Fig. 9 presents the spectral phase angle $\Phi_{u_1u_2}$, along with the u_1- and u_2-spectra, E_{u_1} and E_{u_2}. While E_{u_1} displays one peak at $f^* \approx 0.1$, representing the dominant frequency in the wide wake, E_{u_2} shows one pronounced peak at $f^* \approx 0.3$, as well as one minor peak at $f^* \approx 0.1$, exhibiting the signature of the narrow wake. It may be inferred that u_1 and u_2 are associated with the wide and narrow wakes, respectively. $\Phi_{u_1u_2}$ is calculated from the Fourier transform of the correlation $\overline{u_1(t+\tau)u_2(t)}$. A positive $\Phi_{u_1u_2}$ indicates that u_1 leads u_2, and a negative $\Phi_{u_1u_2}$ means that u_2 leads u_1. $\Phi_{u_1u_2}$ is near zero at $f^* \approx 0.1$, thus corroborating the observation from the LIF data that the gap vortices in the two wakes tend to be in–antiphase. Furthermore, $\Phi_{u_1u_2}$ at $f^* \approx 0.1$ is positive, that is, u_1 leads u_2 at this frequency, implying that the gap vortex in the wide wake generally leads its counterpart in the narrow wake. Let us refocus on Fig. 8. The gap vortex A_0 in the wide wake initially leads B_0 in the narrow wake (Plate 1). A_0 fails to amalgamate with pairing B_0 and C_0 in the narrow wake (Plate 2), perhaps because of an unfavorable phase shift between the two gap vortices. As a matter of fact, A_0 appears lagging behind B_0, deviating from the 'usual' case (Fig. 6) as suggested by $\Phi_{u_1u_2} \approx 0$ at $f^* \approx 0.1$. Subsequently, A_0 grows unusually large in Plate 3 (cf. Fig. 6) but quickly 'squashed' (Plate 4), probably due to the increased interaction with the narrow wake. The collapse of A_0 could momentarily alleviate the interaction between the narrow and the wide wake, allowing the narrow wake to swing towards the wide wake (Plates 4–5). Meanwhile, the weak interaction also encourages the fast growth of the following gap vortex A_1 in the wide wake (Plates 5–6), which collapses again (Plate 7). Similar cycles were repeated. In each cycle, the gap vortex in the wide wake lags behind that in the narrow wake and experiences a rapid growth and then collapses. On the other hand, the gap vortex in the narrow wake became larger and, after three cycles, pushes over the gap flow to the other side (Plates 8), resulting in an upper wide wake and a lower narrow wake. In the whole changeover process, the gap vortex in the wide wake had no chance to amalgamate with the pairing vortices in the narrow wake, probably because of a phase lag behind that in the narrow wake. The observation is consistent with the suggestion that the amalgamation of the three vortices could be important for maintaining the existing narrow and wide wakes (Section 4.2).

In conclusion, the gap vortices in the two wakes tend to be in anti-phase, but the one in the wide wake mostly leads slightly that in the narrow wake and amalgamates with the pairing vortices in the narrow wake. The changeover of the gap flow deflection starts with a phase lag of the gap vortex in the wide wake behind that in the narrow wake. Once lagging behind (compared with antiphase), the gap vortex in the wide wake is prevented from amalgamation with the pairing vortices in the narrow wake and is subsequently likely to grow fast but quickly collapses. The collapse alleviates the interaction between the two wakes, thus allowing the narrow wake to be widened and eventually causing the changeover of the gap flow deflection. The whole process typically needs three to four vortex-shedding cycles in the narrow wake. Speculatively, the 'phase lag' results from interactions between the two wakes. It is therefore not surprising to see the random changeover of gap flow deflection.

4.4. Dominant frequencies

The ratio of the dominant frequency in the narrow wake to that in the wide wake is close to but less than 3 (Kim and Durbin, 1988). The physics behind does not seem to be clear. To gain a better understanding of multiple dominant frequencies, two hot-wires were

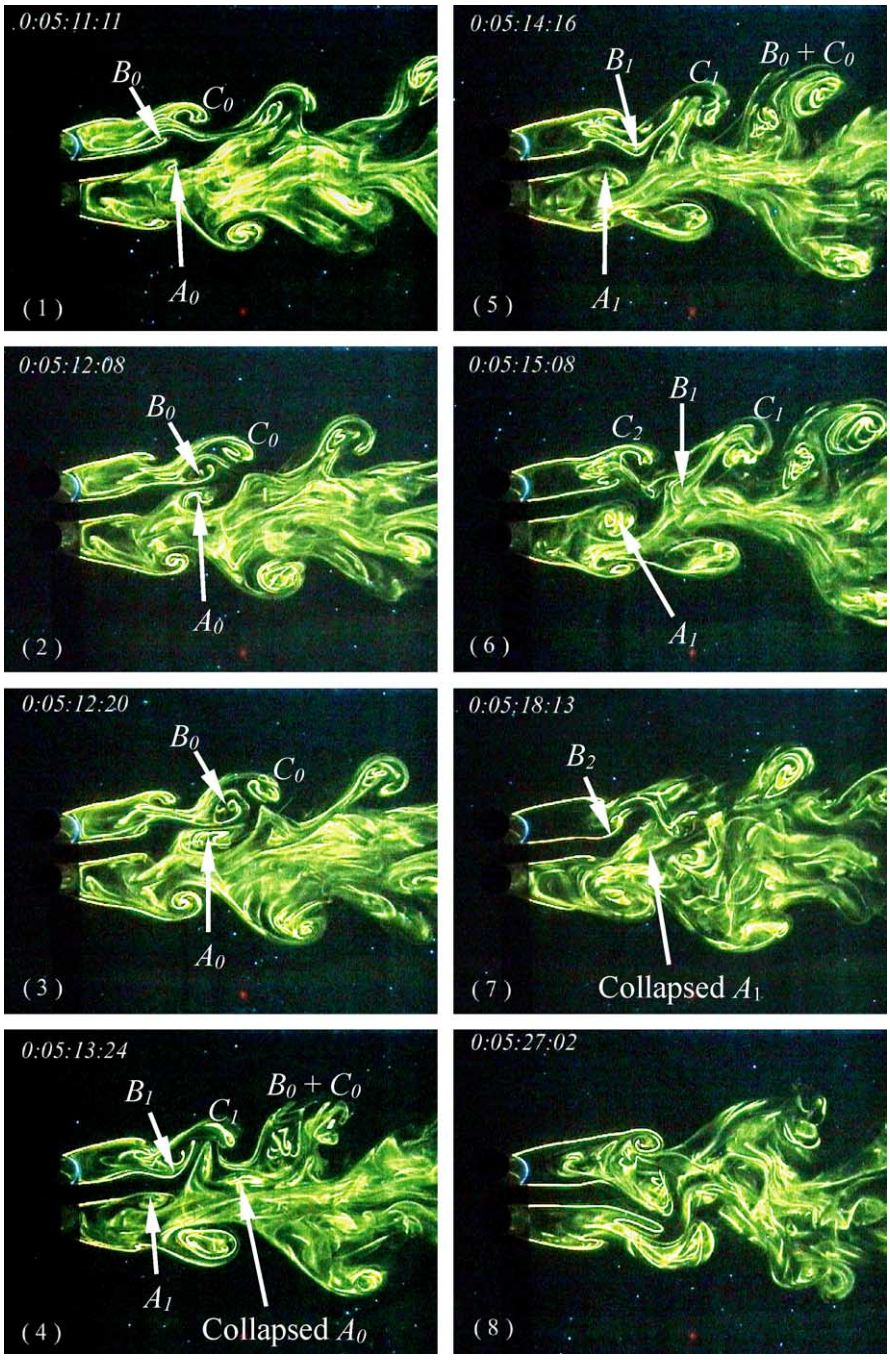

Fig. 8. Sequential photographs from laser-illuminated flow-visualization: the changeover of the gap deflection from one side to another. $T/d = 1.70$. $Re = 230$.

placed symmetrically with respect to $y/d = 0$ at $x/d = 0$ in the two outer shear layers (close to the free-stream), which were associated with the two cylinders, respectively. Fig. 10 presents the power spectrum, E_u, of two simultaneously obtained hot-wire signals, where $\bar{y}/d$ is the distance from the cylinder surface, given by $y/d - 1.35$ for the upper cylinder and $y/d + 1.35$ for the lower cylinder. Two peaks are identifiable at $f^* \approx 0.1$ and 0.3, respectively, in each shear layer, though their strengths are different from one shear layer to the other. For example, the peak at $f^* \approx 0.3$ is more pronounced than that at $f^* \approx 0.1$ in the shear layer associated with the lower cylinder but weaker in the shear layer associated with the upper cylinder.

How to interpret the observed peaks? It is well known that the shear layer separating from a cylinder becomes unstable for $Re > 1000$ and small-scale structures or secondary vortices emerge (Wei and Smith, 1986; Prasad

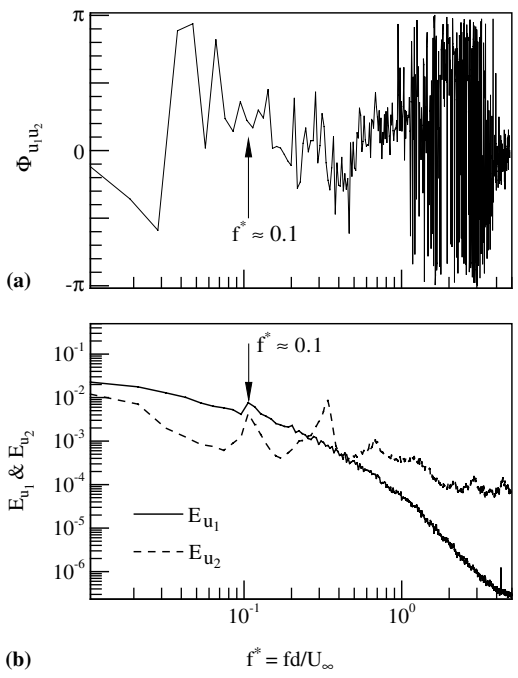

Fig. 9. (a) Spectral phase angles $\Phi_{u_1u_2}$ between simultaneously measured hot-wire signals u_1 at $y/d = 0.4$ and u_2 at $y/d = -0.4 (x/d = 1.5)$; (b) the power spectral density function, E_{u_1} and E_{u_2}, of u_1 and u_2. $T/d = 1.70$.

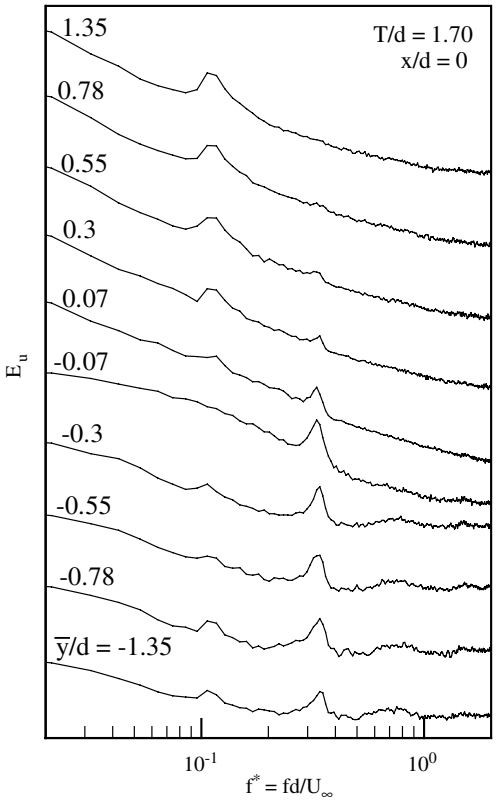

Fig. 10. Power spectrum E_u of the hot-wire signals simultaneously measured in the two outer shear layers associated with the two cylinders. Here $\bar{y}/d$ is the distance from the cylinder surface at $x/d = 0$, given by $y/d - 1.35$ for the upper cylinder and $y/d + 1.35$ for the lower cylinder.

and Williamson, 1997a). The coalescence of the small-scale secondary vortices will increase the scale and reduce the shear layer instability frequency to the Strouhal frequency (Brown and Roshko, 1974; Winant and Browand, 1974; Roshko, 1976; Ongoren and Rockwell, 1988). The secondary vortices are discernible at $Re = 450$ and become evident in present flow visualization for $Re \geqslant 600$. These vortices are seen coalescing to form a larger vortex. Fig. 11 shows sequential photographs from flow visualization. Two small-scale vortices, A_1 and A_2, in Plate 1 are discernible in the narrow wake and approach each other, forming a larger structure (Plates 2–4). Meanwhile, another small-scale vortex, A_3, occurs (Plates 2–4) and catches up with the larger structure (Plates 5–6). They eventually coalesce and roll up into a single vortex in the narrow wake (Plates 7–8). The frequencies of the secondary vortices and the vortices shed from the cylinder in the narrow wake were estimated by means of counting consecutive vortices (about 20 pairs) for a certain period. It is rather difficult to count accurately the secondary vortices and thus estimated normalized frequency scattered over 0.2–0.5. On the other hand the frequency estimate was less scattered for the relatively large-scale vortices shed from the cylinder, ranging from $f^* = 0.10$–0.13 ($Re = 600$). Similar results were obtained for other Re. The observation suggests that vortex shedding be responsible for the peak at $f^* \approx 0.1$ in the narrow wake. In the wide wake, the vortex rolling-up frequency, estimated by counting consecutive vortices on flow-visualization data, is about 0.11 at $Re = 450$, agreeable with that shown in E_u (Fig. 5a).

The peak at $f^* \approx 0.3$ may be connected to the vortex interactions between the two wakes. As discussed in Section 4.2, the two rows of vortices in the narrow wake appear squeezed by the wide wake so that their lateral spacing is very small, thus forming a counter-rotating vortex pair (Fig. 6). It is well known that the anti-parallel vortex pair is prone to reconnection under the effect of the so-called 'Crow instability' (Crow, 1970; Berloff and Roberts, 2001). Furthermore, the two oppositely signed reconnecting vortices draw in the approaching gap vortex in the wide wake. Note that the vortex-shedding frequency in the narrow wake might be the same as the vortex rolling-up frequency in the wide wake. Because of the small lateral spacing between the three vortices, the hot-wire could measure a frequency tripling that in the wide wake.

It is interesting to note that the frequencies of the shear layer instability at $x/d = 0$ are the same as those predominant in the vortex streets downstream. This is not coincidental. Based on published data (Bloor, 1964; Maekawa and Mizuno, 1967; Okamoto et al.,

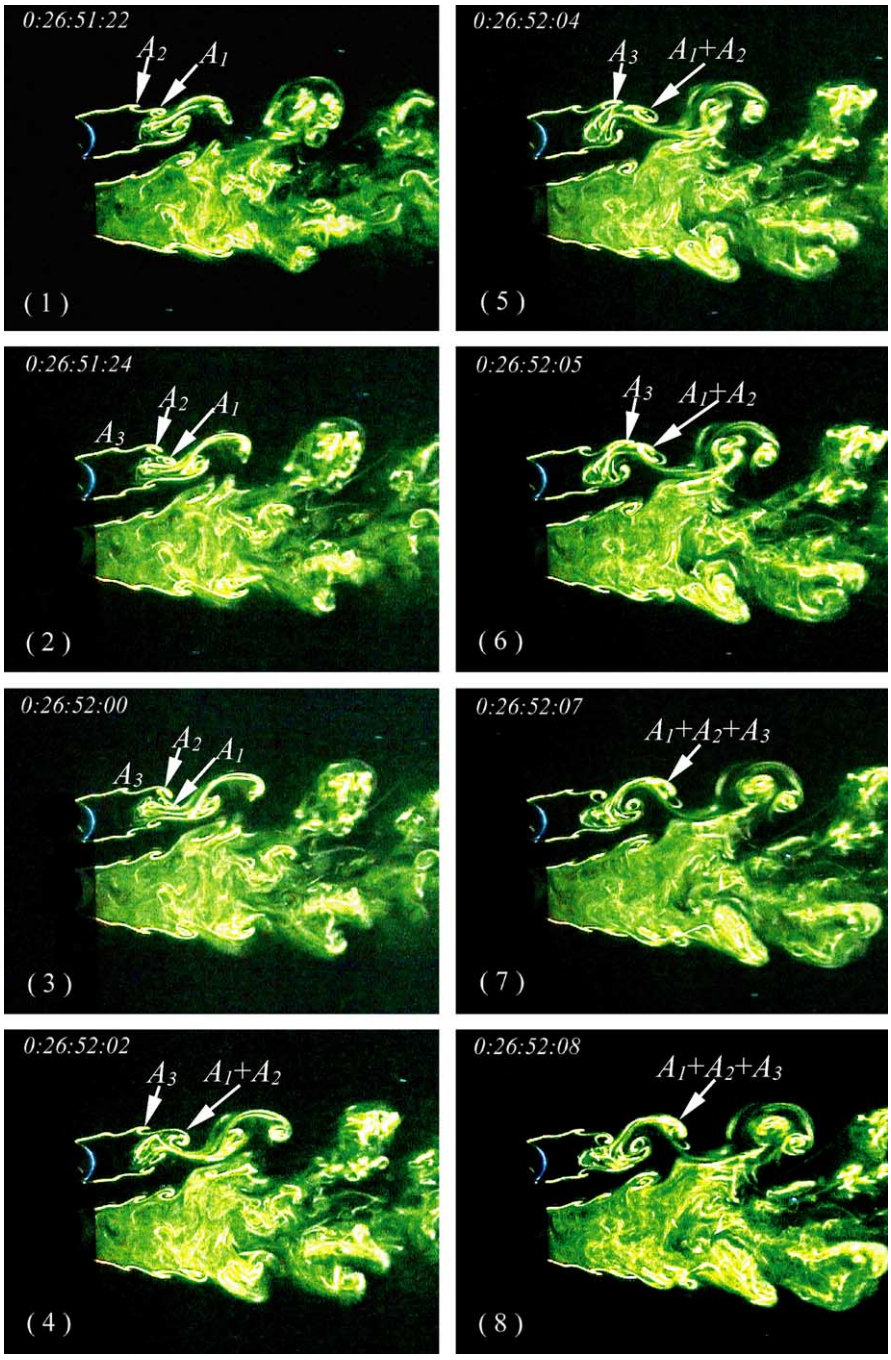

Fig. 11. Sequential photographs from laser-illuminated flow-visualization: the coalescence of the small-scale secondary vortices. $T/d = 1.70$. $Re = 600$.

1981; Wei and Smith, 1986; Kourta et al., 1987; Norberg, 1987) and their own measurement, Prasad and Williamson (1997a) obtained an empirical correlation between Re and the frequency, f_{SL}, of the shear layer instability for a single cylinder in a cross-flow, that is, $f_{SL}/f_S = 0.0235 \times Re^{0.67}$. This correlation would predict $f^*_{SL} = 0.789$ for the present Re (=5900), significantly higher than the measurement (Fig. 10). The deviation is partly due to the fact that the empirical correlation was validated for the range of $Re = 350$–3000, significantly lower than 5900. Although strong interactions between shear layers associated with different cylinders could contribute to the deviation, the upstream influence from the downstream vorticity dynamics should not be overlooked. This influence may have an impact upon the initial evolution of the shear layer instability (Rockwell, 1983; Ho and Huerre, 1984; Michalke, 1984). Roshko (1954) proposed a universal Strouhal number

$St_u = f_s d_w/U_w$. Here d_w is the wake width and $U_w = U_\infty(1 - C_{pw})^{1/2}$, where C_{pw} is the pressure coefficient in the wake. St_u is a constant, about 0.16 in a single cylinder wake. The Strouhal number St was then written as $St = St_u \frac{d}{d_w}(1 - C_{pw})^{1/2}$. Evidently, d_w or the shear layer thickness and St are inversely related. Presumably, this relationship is also qualitatively valid in the wide wake, implying that the vortical structure frequency $f^* \approx 0.1$ might be dictated by the shear layer thickness. This frequency may feed back upstream and be probably responsible for the peak at $f^* \approx 0.1$ in E_u (Fig. 5) measured in the shear layers around the cylinders.

As proposed earlier, the peak at $f^* \approx 0.3$ in the hot-wire spectrum may be connected to the amalgamation of three vortical structures. This frequency could feed back upstream and excite the shear layer instability. Note that once anti-parallel vortex pair starts reconnecting, the circulation of each vortex decreases rapidly due to the reorientation of vorticity (Leweke and Williamson, 1998). Accordingly, the three structures should be weakened in strength, compared with that in the wide wake, due to vorticity cancellation. This is indeed confirmed in Fig. 5b; the peak at $f^* \approx 0.3$ in the narrow wake is considerably reduced at $x/d = 5$. Consequently, the peak in the spectrum E_u (Fig. 10) at $f^* \approx 0.1$ is significant in the shear layers associated with both cylinders, whereas the peak at $f^* \approx 0.3$ is not so evident in the shear layer associated with the cylinder, which is relatively far away and responsible for the generation of the wide wake.

In conclusion, as being inferred previously in Section 4.1, the vortical structures in the wide wake may originate from rolling-up under the effect of the wake shear layer instability. Its frequency is therefore dictated by the shear layer thickness, say $f^* \approx 0.1$ (e.g. Fig. 7). This frequency could feed back upstream to excite the shear layer instability and further induce vortex shedding in the narrow wake at $f_s^* \approx 0.1$. It is proposed that the uncompleted amalgamation (Fig. 6) of two cross-stream vortices in the narrow wake and the gap vortex in the wide wake could be responsible for the dominant frequency 0.3 in the hot-wire spectrum in the narrow wake (e.g. Fig. 5). It should be emphasized that this proposition has yet to be verified in future investigations.

5. Role of gap bleeding for small cylinder spacing

At $T/d = 1.13$, there is no vortex generated in the gap between the two cylinders and vortices are generally shed alternately from the free-stream sides of the cylinders, thus generating a single vortex street (Fig. 12). This was confirmed by the PIV measurement at $Re = 5900$ (not shown). The behavior of gap bleeding is quite different between the laminar and turbulent flows. Gap bleeding appeared swerving almost around the cylinder in the laminar case (Fig. 12a), but it is biased to a lesser degree in the turbulent case (Fig. 12b), possibly due to higher momentum or inertia. The higher momentum of gap bleeding is also likely responsible for the prolonged vortex formation region (Sumner et al., 1999). Gap bleeding may change its deflection from time to time. This type of gap flow unsteadiness may lead to a lower frequency in the near-wake of a normal plate (e.g. Najjar and Balachandar, 1998). A test was presently conducted using hot-wires to estimate the time interval for gap bleeding to change its deflection from one side to the other. Six changes, as indicated by a jump in the hot-wire signal level, were recorded at $T/d = 1.13$ for $Re = 5900$ during 5 min, suggesting that its frequency is of several orders lower than that of vortex shedding. Naturally, such a low-frequency component was not observed in the hot-wire spectrum based on the data obtained at a sampling frequency of 6.0 kHz and the duration of 20 s (Section 2.2). Note that only one changeover of the gap flow deflection was observed in 5 min for $T/d = 1.70$. It is evident that the gap flow deflection is less stable at $T/d = 1.13$ than at $T/d = 1.70$.

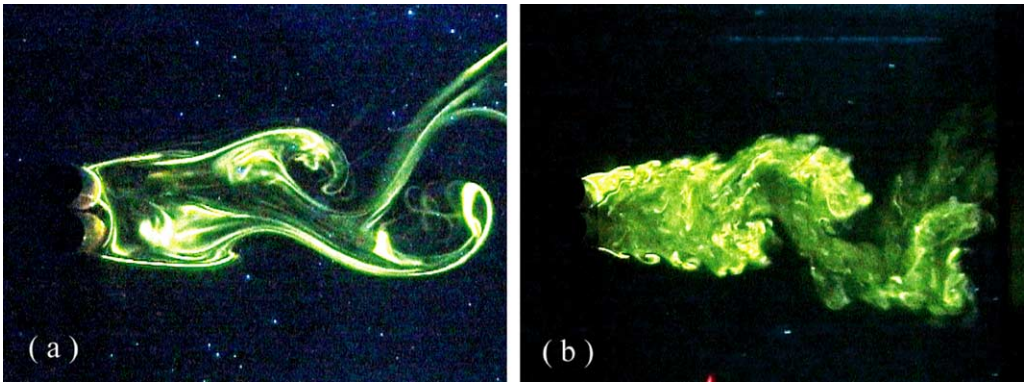

Fig. 12. Typical flow patterns at $T/d = 1.13$. (a) $Re = 150$; (b) $Re = 750$.

Symmetric vortex shedding (Plate 1 in Fig. 13) occurs occasionally, which is associated with unbiased gap bleeding. This mode of the flow structure is unstable and in general quickly reverts to the alternate vortex-shedding mode, which corresponds to a deflected gap bleeding. Due to the interaction between vortices, the symmetric arrangement of vortices is less stable than the anti-symmetric arrangement (Goldstein, 1965); even in the symmetric vortex-shedding case, vortices downstream still exhibit an anti-symmetrical spatial arrangement. Fig. 13 presents sequential photographs at $Re = 250$ in order to gain a better understanding of the relationship between gap bleeding and the near-wake vortex pattern. Initially, the gap flow was not deflected and two vortices, as marked by arrows in Plate 1, started to form on the free-stream sides of the two cylinders, respectively, in a symmetrical manner. As they move downstream, vortex rolling-up from the lower cylinder appears traveling faster than not only its counterpart from the upper cylinder but also the one shed earlier from the same cylinder (Plates 2–3). As a result, the two consecutive vortices of the same sign merged, forming a larger structure (see Plates 4–5). On the other hand, the symmetrically formed upper vortex fell behind. Meanwhile, two more vortices following started to roll up symmetrically (Plates 4 and 5). The upper one appears moving fast and merging with the one of the same sign, shed earlier (Plates 6 and 7). Eventually, an anti-symmetrical spatial arrangement occurs (Plates 7–9). Note that gap bleeding starts to deflect and anti-symmetric vortex-shedding resumes.

Sumner et al. (1999) suggested that for $T/d < 1.2$ gap bleeding was usually associated with higher momentum, acting to increase the streamwise extent of the vortex formation region. They noted that alternate vortex shedding was supplanted from time to time by symmetric shedding. The present flow-visualization data unveil that alternate vortex shedding is associated with a biased gap bleeding, while symmetric shedding corresponds to an unbiased bleeding. The bleeding effect persists at least up to $x/d = 10$, resulting in an asymmetrical vortex street about the flow centerline and the asymmetrical cross-stream distributions of mean velocity and Reynolds stresses (not shown). This is in distinct contrast with the wake of a single cylinder, where mean velocity and Reynolds stresses are symmetrical or anti-symmetrical about the centerline (Zhou and Antonia, 1993). Evidently, the role the gap bleeding plays in the vortex for-

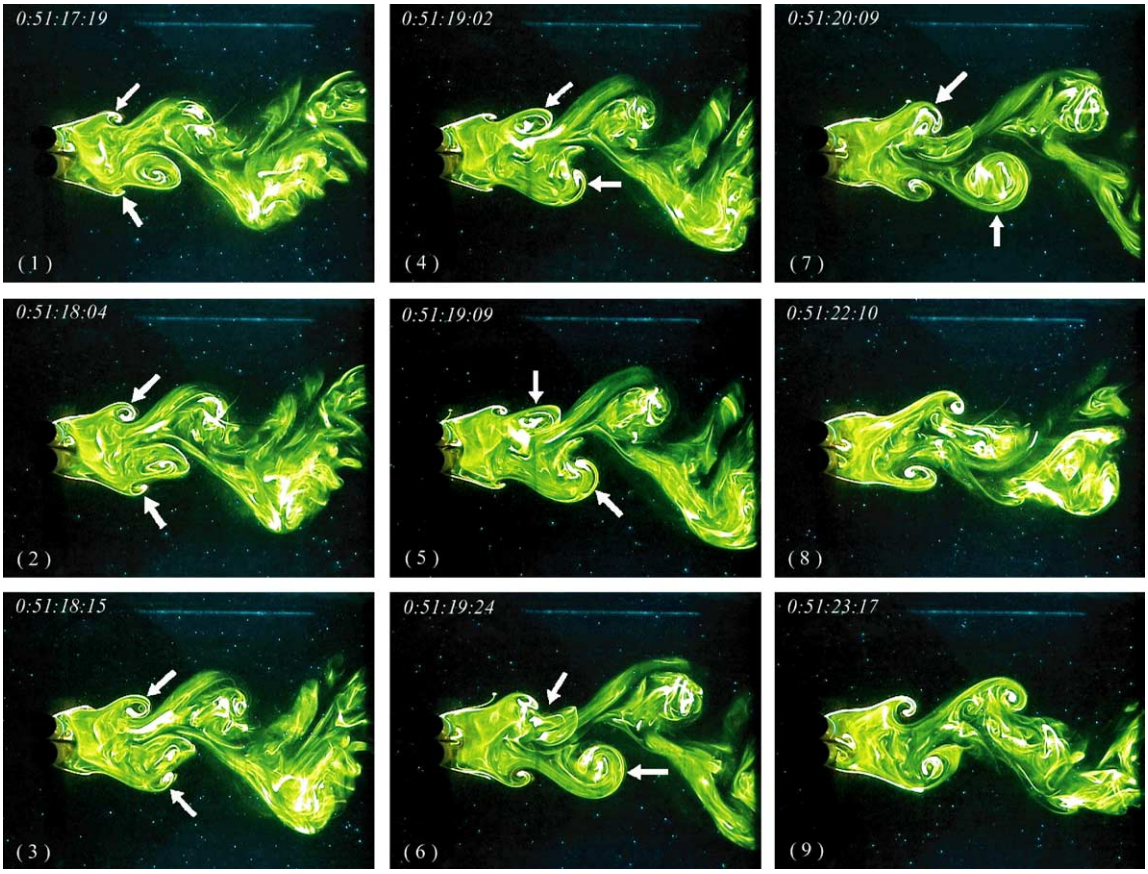

Fig. 13. Sequential photographs from laser-illuminated flow-visualization: transition from the symmetric to anti-symmetric vortex shedding at $T/d = 1.13$ ($Re = 250$).

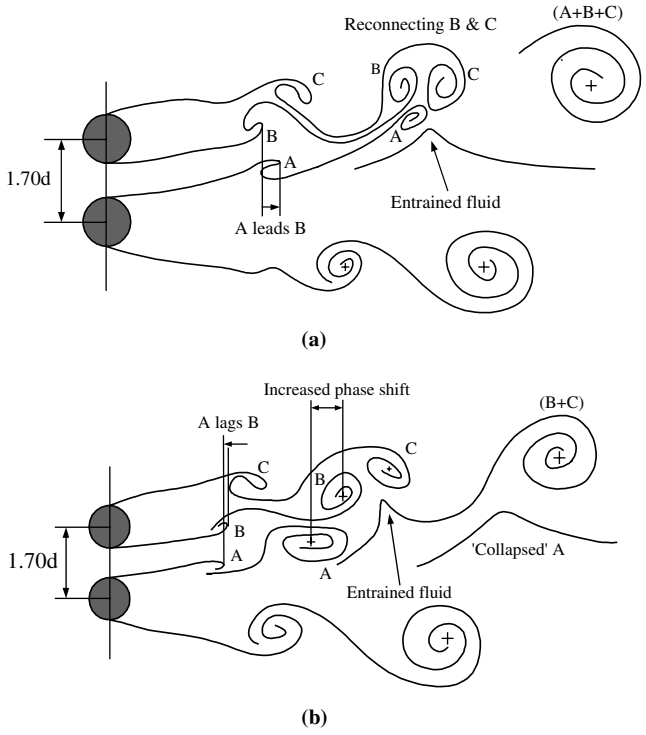

Fig. 14. Summary sketch for the vortex formation and evolution behind two side-by-side circular cylinders in the asymmetrical flow regime. (a) Stably deflected gap flow is associated with the amalgamation of the two reconnecting opposite-sign vortices in the narrow wake with the gap vortex in the wide wake. (b) Changeover of the gap flow deflection begins with the gap vortex in the wide wake lagging behind that in the narrow wake. In both cases, an asymmetrical single vortex street occurs downstream.

mation cannot be neglected, which is probably the essence of difference between a single bluff body and the two cylinders of small spacing.

6. Concluding remarks

At large cylinder spacing, i.e. $T/d = 3.00$, predominantly anti-phase vortex shedding from the two cylinders changes from time to time to in-phase vortex shedding. The change starts with a slight phase deviation from anti-phase vortex shedding from the two cylinders. The subsequent interactions between the two streets lead to the formation of in-phase vortex shedding from the two cylinders and hence the in-phase mode streets. However, in-phase vortex shedding is unstable and soon returns to the anti-phase manner (Fig. 3).

As the two cylinders approach each other, interactions between the two vortex streets are intensified, resulting in a totally different flow structure. Fig. 14 summarizes typical flow patterns, sketched following streak lines in the photographs of flow visualization at $T/d = 1.70$. The bi-stability appears linked with interactions among gap vortices A, B and C. A and B are in general in anti-phase. Mostly, A leads B (Fig. 14a). In this case, the two cross-stream vortices in the narrow wake are typically engaged in pairing, and may generate a relatively low-pressure region between them, thus drawing in fluid as well as the gap vortex in the wide wake. It is inferred that the amalgamation of the three vortices could be, at least partly, responsible for the stability of the gap flow deflection, i.e., maintaining the narrow and wide wake. Based on the streamwise evolution of the hot-wire signal spectrum (Fig. 5), the amalgamation completes probably before $x/d = 10$, which implies the merging of the two wakes or a single vortex street further downstream. The two rows of vortices in the new street are likely to be different in many aspects such as in size and vorticity strength because of different formation processes involved. The assertion conforms to the report by Zhou et al. (2002), who observed a single asymmetrical vortex street ($T/d = 1.5$, $Re = 5800$) at $x/d = 10$–40 based on phase-averaged velocity and temperature fields.

The changeover of the gap flow deflection starts with a phase lag of the gap vortex in the wide wake behind that in the narrow wake. Once A lags behind B, the phase difference between them is likely to increase as they travel downstream. As a result, A fails to amalgamate with the pairing vortices B and C in the narrow wake (Fig. 14b). This could destabilize the gap flow deflection and give rise to its changeover. Indeed, A tends to grow in size but quickly collapses because of the increased interaction with the narrow wake, thus alleviating momentarily interactions between the two wakes and allowing the narrow wake to expand laterally. The process is likely to repeat for a few vortex-shedding cycles and eventually the narrow wake pushes the gap flow to the other side and completes the changeover.

Two dominant frequencies, i.e. $f^* \approx 0.1$ and 0.3, are detected in the outer shear layer associated with each cylinder. The two frequencies were also identifiable in the narrow wake, but the lower frequency 0.1 only was detected in the wide wake. Flow-visualization data suggest that vortex shedding occurs at $f_s^* \approx 0.1$ in the narrow wake. The shedding frequency coincides with the rolling-up frequency of the vortical structures in the wide wake. Presumably, the vortex frequency in the wide wake is dictated by the shear layer thickness. This frequency could feed back upstream to excite the shear layer instability and further induce vortex shedding in the narrow wake. On the other hand, the amalgamation of two cross-stream vortices in the narrow wake and the gap vortex in the wide wake leads to reduced lateral spacing between the structures. It is speculated that the laterally approaching three structures could be responsible for the dominant frequency 0.3 in the hot-wire spectrum. The upstream influence of this frequency could excite the shear layer instability, thus resulting in a dominant frequency at $f^* \approx 0.3$.

At $T/d = 1.13$, there are no gap vortices generated and vortices are shed only from the free-stream side of the two cylinders, resulting in a single vortex street. This flow is however different from that behind a single bluff body. Gap bleeding between the cylinders plays a significant role in determining the flow pattern behind the cylinders. Gap bleeding is mostly biased towards one cylinder, which corresponds to alternate vortex shedding from the free-stream side of the two cylinders. When the bleeding is unbiased, symmetric vortex shedding occurs.

Acknowledgment

YZ wishes to acknowledge support given to him by the Research Grants Council of the Government of the HKSAR through Grants PolyU5316/03E.

References

Bearman, P.W., Wadcock, A.J., 1973. The interference between a pair of circular cylinders normal to a stream. Journal of Fluid Mechanics 61, 499–511.

Berloff, N.G., Roberts, P.H., 2001. Motion in a Bose condensate: IX Crow instability of antiparallel vortex pairs. Journal of Physics A: Mathematical and General 34, 10057–10066.

Bloor, M.S., 1964. The transition to turbulence in the wake of a circular cylinder. Journal of Fluid Mechanics 19, 290–304.

Brown, G.L., Roshko, A., 1974. On density effects and large-scale structure in turbulent mixing layers. Journal of Fluid Mechanics 64, 775–816.

Crow, S.C., 1970. Stability theory for a pair of trailing vortices. AIAA Journal 8 (12), 2172–2179.

Englar, R.J., 1975. Circulation control for high-lift and drag generation on STOL aircraft. Journal of Aircraft 12, 457–464.

Goldstein, S., 1965. Modern Developments in Fluid Dynamics. Dover Publications, New York, USA. Vol. 1, pp. 59–65; Vol. 2, pp. 417–418.

Granger, S., Campistron, R., Lebret, J., 1993. Motion-dependent excitation mechanisms in a square in-line tube bundle subject to water cross-flow: an experimental modal analysis. Journal of Fluids and Structures 7, 521–550.

Ho, C.M., Huerre, P., 1984. Perturbed free-shear layers. Annual Review of Fluid Mechanics 16, 365–424.

Ishigai, S., Nishikawa, E., Nishmura, K., Cho, K., 1972. Experimental study on structure of gas flow in tube banks with tube axes normal to flow (Part 1, Karman vortex flow around two tubes at various spacings). Bulletin of the JSME 15, 949–956.

Kamemoto, K., 1976. Formation and interaction of two parallel vortex streets. Bulletin of the JSME 19, 283–290.

Kim, H.J., Durbin, P.A., 1988. Investigation of the flow between a pair of circular cylinders in the flopping regime. Journal of Fluid Mechanics 196, 431–448.

Kiya, M., Arie, M., Tamura, H., Mori, H., 1980. Vortex shedding from two circular cylinders in staggered arrangement. Journal of Fluids Engineering 102, 166–173.

Kolář, V., Lyn, D.A., Rodi, W., 1997. Ensemble-averaged measurements in the turbulent near wake of two side-by-side square cylinders. Journal of Fluid Mechanics 346, 201–237.

Kourta, A., Boisson, H.C., Chassaing, P., Ha Minh, H., 1987. Nonlinear interaction and the transition to turbulence in the wake of a circular cylinder. Journal of Fluid Mechanics 181, 141–161.

Kumada, M., Hiwada, M., Ito, M., Mabuchi, I., 1984. Wake interference between three circular cylinders arranged side by side normal to a flow. Transactions of JSME 50, 1699–1707 (in Japanese).

Landweber, L., 1942. Flow about a pair of adjacent, parallel cylinders normal to a stream. D.W. Taylor Model Basin, Department of the Navy, Report 485, Washington, DC.

Leweke, T., Williamson, C.H.K., 1998. Cooperative elliptic instability of a vortex pair. Journal of Fluid Mechanics 360, 85–119.

Maekawa, T., Mizuno, S., 1967. Flow around the separation point and in the near-wake of a circular cylinder. Physics of Fluids (Suppl. S184).

Meneghini, J.R., Saltara, F., 2001. Numerical simulation of flow interference between two circular cylinders in tandem and side-by-side arrangements. Journal of Fluids and Structures 15, 327–350.

Michalke, A., 1984. Survey on jet instability theory. Progress in Aerospace Sciences 21, 159–199.

Moretti, P., 1993. Flow-induced vibration in arrays of cylinders. Annual Review of Fluid Mechanics 25, 99–114.

Najjar, F.M., Balachandar, S., 1998. Low-frequency unsteadiness in the wake of a normal flat plate. Journal of Fluid Mechanics 370, 101–147.

Ng, C.W., Cheng, V.S.Y., Ko, N.W.M., 1997. Numerical study of vortex interactions behind two circular cylinders in bistable flow regime. Fluid Dynamics Research 19, 379–409.

Norberg, C., 1987. Effect of Reynolds number and a low-intensity freestream turbulence on the flow around a circular cylinder. Publ. 87/2. Dept. Applied Thermodynamics and Fluid Mechanics, Chalmers University of Technology.

Okamoto, S., Hirose, T., Adachi, T., 1981. The effect of sound on the vortex-shedding from a circular cylinder. Bulletin of the JSME 24, 45–53.

Ongoren, A., Rockwell, D., 1988. Flow structure from an oscillating cylinder: Part 1. Mechanisms of phase shift and recovery in the near wake. Journal of Fluid Mechanics 191, 197–223.

Prasad, A., Williamson, C.H.K., 1997a. The instability of the shear layer separating from a bluff body. Journal of Fluid Mechanics 333, 375–402.

Prasad, A., Williamson, C.H.K., 1997b. Three-dimensional effects in turbulent bluff-body wakes. Journal of Fluid Mechanics 343, 235–265.

Rockwell, D., 1983. Invited lecture: oscillations of impinging shear layer. AIAA Journal 21, 645–664.

Roshko, A., 1954. On the drag and shedding frequency of bluff cylinders. Nat. Adv. Comm. Aero., Wash., Tech. Note 3169.

Roshko, A., 1976. Structure of turbulent shear flows: a new look. AIAA Journal 14, 1349–1357.

Sobey, I.J., 2000. Introduction to Interactive Boundary Layer Theory. Oxford University Press, Oxford, New York, pp. 284–298.

Spivac, H.M., 1946. Vortex frequency and flow pattern in the wake of two parallel cylinders at varied spacing normal to an air stream. Journal of the Aeronautical Sciences 13, 289–301.

Sumner, D., Price, S.J., Païdoussis, M.P., 2000. Flow-pattern identification for two staggered circular cylinders in cross-flow. Journal of Fluid Mechanics 411, 263–303.

Sumner, D., Wong, S.S.T., Price, S.J., Païdoussis, M.P., 1999. Fluid behaviour of side-by-side circular cylinders in steady cross-flow. Journal of Fluids Structures 13, 309–338.

Weaver, D.S., Abd-Rabbo, A., 1984. A flow visualization study of a square array of tubes in water cross-flow. In: Paidoussis, M.P., Au-Yang, M.K., Chen, S.S. (Eds.), Proceedings Symposium on Flow-Induced Vibrations, vol. 2, pp. 165–177.

Wei, T., Smith, C.R., 1986. Secondary vortices in the wake of circular cylinders. Journal of Fluid Mechanics 169, 513–533.

Williamson, C.H.K., 1985. Evolution of a single wake behind a pair of bluff bodies. Journal of Fluid Mechanics 159, 1–18.

Williamson, C.H.K., 1996. Vortex dynamics in the cylinder wake. Annual Review of Fluid Mechanics 28, 477–539.

Winant, C.D., Browand, F.K., 1974. Vortex pairing, the mechanism of turbulent mixing layer growth at moderate Reynolds number. Journal of Fluid Mechanics 63, 237–255.

Xu, S.J., Zhou, Y., So, R.M.C., 2003. Reynolds number effects on the flow structure behind two side-by-side cylinders. Physics of Fluids 15, 1214–1219.

Zdravkovich, M.M., 1977. Review of flow interference between two circular cylinders in various arrangements. Journal of Fluids Engineering 99, 618–633.

Zdravkovich, M.M., 1985. Flow-induced oscillations of two interfering circular cylinders. Journal of Sound and Vibrations 101, 511–521.

Zhang, H.J., Zhou, Y., 2001. Effect of unequal cylinder spacing on vortex streets behind three side-by-side cylinders. Physics of Fluids 13 (12), 3675–3686.

Zhou, Y., Antonia, R.A., 1993. A study of turbulent vortices in the wake of a cylinder. Journal of Fluid Mechanics 253, 643–661.

Zhou, Y., Antonia, R.A., 1994. Effect of initial conditions on structures in a turbulent near-wake. AIAA Journal 32, 1207–1213.

Zhou, Y., Antonia, R.A., Tsang, W.K., 1998. The effect of the Reynolds number on a turbulent far-wake. Experiments in Fluids 25, 118–125.

Zhou, Y., Wang, Z.J., So, R.M.C., Xu, S.J., Jin, W., 2001. Free vibrations of two side-by-side cylinders in a cross-flow. Journal of Fluid Mechanics 443, 197–229.

Zhou, Y., Zhang, H.J., Yiu, M.W., 2002. The turbulent wake of two side-by-side circular cylinders. Journal of Fluid Mechanics 458, 303–332.